International Journal of Nanomedicine

Dovepress
open access to scientific and medical research

Open Access Full Text Article

ORIGINAL RESEARCH

# A Double-Chamber "Dandelion" Appearance Sequential Drug Delivery System for Synergistic Treatment of Malignant Tumors

Jian Li[1–3], Qing Zhang[1–3], Jiahui Cai[1–3], Yibo Yang[1–3], Jia Zhang[1–3], Yanting Gao[1–3], Shihe Liu[1–3], Kun Li[1–3], Ming Shi[1–3], Zhiwei Liu[1–3], Liming Gao[4]

[1]College of Environmental & Chemical Engineering, Yanshan University, Qinhuangdao, People's Republic of China; [2]Applied Chemistry Key Laboratory of Hebei Province, Yanshan University, Qinhuangdao, People's Republic of China; [3]Key Laboratory of Nanobiotechnology of Hebei Province, Yanshan University, Qinhuangdao, People's Republic of China; [4]Oncology Department, the First Hospital of Qinhuangdao, Qinhuangdao, People's Republic of China

Correspondence: Jian Li, College of Environment & Chemical Engineering, Yanshan University, No. 438 Hebei Street, Qinhuangdao, 066004, People's Republic of China, Tel +86-335-8061569, Fax +86-335-8061569, Email Lijianbio@ysu.edu.cn



**Introduction:** During the combined treatment of tumors, the non-interfering transportation of drugs with different solubilities and the controllable sequential release are the main challenges. Here, we reported a double-chamber "Dandelion" -like sequential drug delivery system to realize the sequential release of different drugs for treating malignant tumors synergistically.

**Methods:** After synthesizing mesoporous silica nanoparticles (MSN) by template method, a hydrophilic chemotherapy drug doxorubicin (DOX) was loaded into the channels of mesoporous silica (MSN) and locked with polydopamine (PDA) coating. Next, β-cyclodextrin (β-CDs) was decorated on PDA by Michael addition reaction, and the hydrophobic photosensitizer chlorin e6 (Ce6) was encapsulated into the hydrophobic chambers of β-CDs. Finally, AS1411 was modified on the surface of PDA and obtained DOX@MSN@PDA-β-CD/Ce6-AS1411 nanoparticles (DMPCCA) through which orthogonal loading and effective controlled release of different drugs were realized.

**Results:** Under the sequential irradiations of 808 nm and 660 nm near-infrared (NIR) laser, PDA promoted the extensive release of Ce6 firstly while playing the effect of photothermal therapy (PTT), further to achieve the effect of photodynamic therapy (PDT) of Ce6. Meanwhile, the rapid release of DOX loaded in MSN channels showed a time lag of about 5 h after Ce6 release, through which it maximized the chemotherapeutic effect. Besides, the present drug loading nano-platform combined passive tumor-targeting effect given by EPR and active tumor-targeting effect endowed by AS1411 realized PTT-PDT-chemotherapy triple mode synergistic combination.

**Conclusion:** We offer a general solution to address the key limitations for the delivery and sequential release of different drugs with different solubilities.

**Keywords:** sequential release, mesoporous silica, chemotherapy, tumor-targeting, PTT-PDT-chemotherapy combination

## Introduction

Pernicious tumors have the characteristics of rapid growth, easy metastasis, and recurrence, which seriously threatens human life and health. Advanced therapies to eliminate primary tumors and inhibit tumor metastasis are the ultimate goals in the battle against cancers.[1,2]

Nowadays, chemotherapeutic drugs are widely used in tumor treatments. Single chemotherapy always leads to severe adverse effects and drug resistance which limit therapeutic efficacy.[3] Therefore, multimodal therapy involving multiple action mechanisms has received extensive attention, such as photodynamic therapy (PDT), photothermal therapy (PTT), chemodynamical therapy (CDT), gene therapy (GT), and starvation therapy (ST).[4] Among them, PTT and PDT have been studied most deeply and have shown clinical impacts in a variety of tumors. PTT exhibits the outstanding advantages of less toxic and side effects, good temporal and spatial selectivity, fast postoperative recovery, and high

Received: 7 April 2022
Accepted: 29 August 2022
Published: 1 September 2022

**Graphical Abstract**

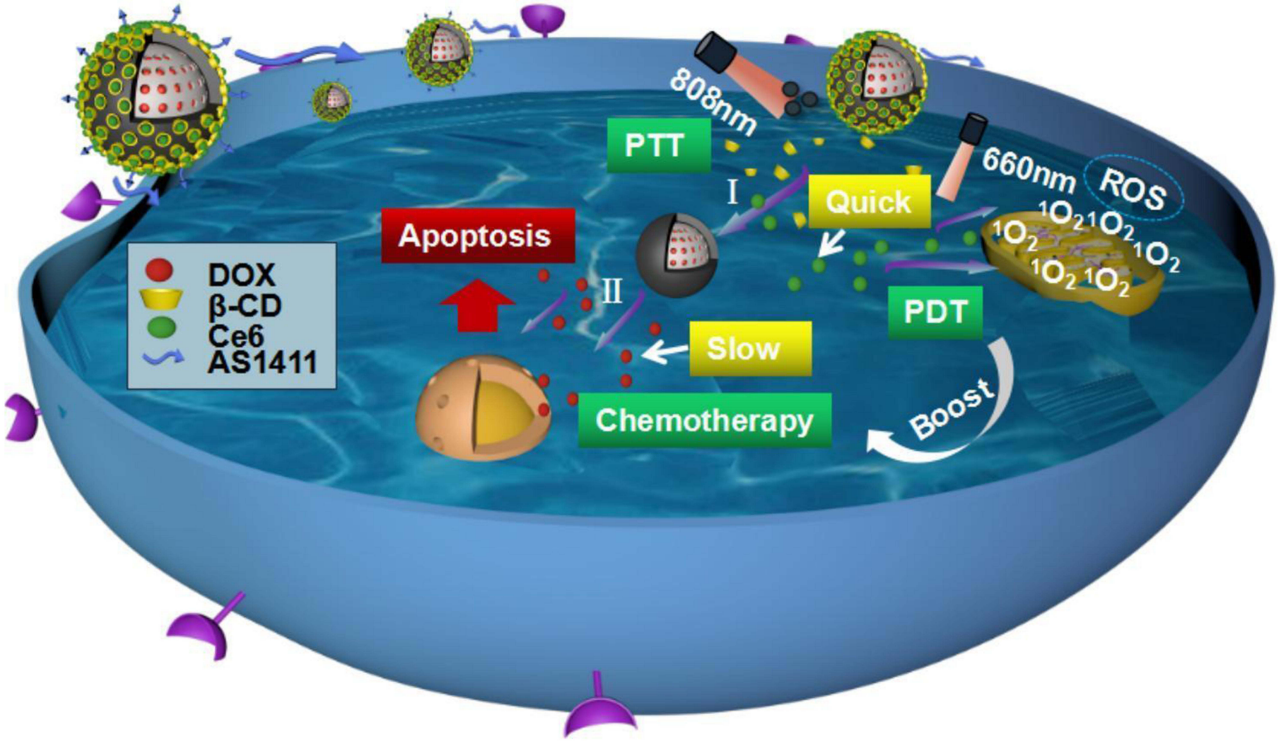


efficiency. PDT can produce high levels of reactive oxygen species (ROS) through the incomplete reduction of oxygen after light irradiation mediated by photosensitizers (PS), and causes effective vascular and tumor cell damages.[5]

However, at present, there are still some problems that cannot be ignored in the combined treatment of multiple drugs. There are many problems when a variety of drugs with different solubilities are loaded into the same cavity at the same time, such as the reduction of drug loading, the interference between drugs, and even the difficulty of realizing the spatio-temporal controlled release of different drugs. However, sequential release (SR) delivery systems are usually based on a series of different microcarriers or nanocarriers, which are uniquely characterized by the ability to release one or more drugs in a controlled sequence at different times or locations.[6] SR delivery system improves the tumor microenvironment by releasing one drug in advance, so that the drugs released later can play a more effective role and achieve more effective synergy between drugs.[7]

Therefore, an ideal drug delivery system with double cavities needs to be constructed to achieve 1) efficient loading of two drugs with different solubilities, and 2) sequential release of different drugs to realize better synergy between drugs. One type of cavity can be provided by mesoporous silica nanoparticles (MSN), which are considered to be an ideal carrier with the characteristics of low biological toxicity, high loading efficiency of hydrophilic drugs, sustainable release of anticancer drugs, and easy surface modification and manufacture.[8,9] Also, MSN has been employed for the construction of ideal spatiotemporal drug release system.[10,11] In order to achieve the on-demand drug delivery, mesoporous silica nanocarriers usually need to be gated with stimulus-responsive capping agents. Because polydopamine (PDA) possessed acidic stimulation response, it can be wrapped on the surface of MSN as a sealing layer to avoid drug leakage during the internal circulation. Moreover, PDA displays ideal photothermal properties, which can convert light energy into heat energy for photothermal treatment of tumors, and can also accelerate molecular motion.[12,13] This greatly improves the possibility of practical application of this monodisperse silica system in vivo cancer treatment.[14] The other type of cavity can be offered by β-cyclodextrin (β-CD). It is the cyclic oligosaccharide which has, respectively, composed of 6, 7 or 8 glucose units, formed by α-1,4 glycosidic bond and has a hollow truncated cone structure in space.[15] The inner cavity of β-CD is micro hydrophobic and hydrophobic drugs can be

encapsulated in the cavity of cyclodextrin through non-covalent interaction to form inclusion complexes without complex chemical reactions.[16]

Based on the above thinking, a double-cavity nanocarrier was synthesized for loading hydrophilic chemo-therapeutic drug doxorubicin (DOX) and hydrophobic photosensitizer chlorine 6 (Ce6) for PDT in our study. Under near-infrared (NIR) laser irradiation, PDA is induced to generate the hyperthermia effect of tumor cells and trigger the ultrafast release of Ce6 in tumor cells. A high concentration of ROS produced by photosensitizer-mediated photodynamic therapy effectively inhibits P-glycoprotein (p-gp), further increasing the sensitivity of multidrug resistance (MDR) cells to chemical drugs. Compared with the simultaneous release of these two kinds of drugs, the antitumor efficacy of sequential release of Ce6 and DOX will be significantly improved.[17–19]

Nanoparticles with appropriate size not only achieve passive targeting through the EPR effect but also further increase their active tumor targeting if their surface is functionalized with some antibodies or nucleic acid aptamers against tumor cell-specific antigens.[20] Aptamer AS1411 is a kind of aptamer with a strong affinity for nucleolin specifically expressed on the surface of tumor cells and has been widely used as the target motif of antitumor drug or contrast agent delivery systems.[21] Our previous study also illustrated the specific binding effect of AS1411 for HeLa cells.

In this study, we engineered a double-chamber drug delivery system named DOX@MSN@PDA-β-CD/Ce6-AS1411 (DMPCCA) to realize sequential release of drugs with different action mechanisms for treating malignant tumors synergistically. A hydrophilic chemotherapy drug DOX was loaded into the channels of MSN and locked with PDA coating. Furthermore, after the decoration of HS-β-CDs on PDA by Michael addition reaction between catechol and sulfhydryl group,[22,23] the hydrophobic photosensitizer Ce6 was encapsulated into the hydrophobic chambers of β-CDs, through which orthogonal loading and effective controlled release of different drugs were realized (Scheme 1A). Through the EPR effect produced by the particle size of 180–200 nm and the binding ability of AS1411 to nucleolin on the surface of tumor cell membrane, the nanoparticles accumulated near tumor cells. After entering tumor cells through endocytosis, β-CDs in the outer layer were degraded, and Ce6 was released under lysosomal acid conditions and accelerated by the thermal generated by PDA photothermal conversion. Under 660 nm NIR irradiation, ROS was generated through oxygen consumption, which promoted lysosomal escape of drugs and improved tumor microenvironment for the later released chemotherapeutic drug DOX to play its role. At the same time, PDA coating also produced photothermal conversion under 880 nm NIR laser irradiation to realize PTT. Subsequently, PDA coating was decomposed in an acidic environment, and DOX was released to further play the role of chemotherapy. This drug delivery system loads drugs with different solubilities and releases them successively (Scheme 1B).

# Materials and Methods

## Materials

Cetyltrimethylammonium bromide (CTAB), sodium hydroxide, tetraethyl silicate (TEOS), Ce6 and HS-β-cyclodextrin (HS-β-CD) were provided by Sigma–Aldrich (USA). AS1411-$NH_2$ (5′-$NH_2$-TTGGTG GTG GTG GTT GTG GTG GTG GTG G-3′) was purchased from Sangon Biotech (Shanghai, China). 1,3-diphenylisobenzofuran (DPBF) was purchased from Alladin Reagent Company (Shanghai, China). Calcein/PI Cell Viability/Cytotoxicity Assay Kits were purchased from Yaji Biotech (Shanghai, China). Fetal bovine serum (FBS) and Dulbecco's Modified Eagle Medium (DMEM) were purchased from Gibco (NY, USA). Penicillin and streptomycin were obtained from Thermo Science (Beijing, China). CCK-8 Assay Kits, Reactive Oxygen Species Assay Kits, and blood urea nitrogen (BUN), creatinine (CRE), alanine aminotransferase (ALT), and aspartate transaminase (AST) assay kits were all purchased from Abcam (Shanghai, China). Terminal deoxynucleotidyl transferase dUTP nick-end labeling (TUNEL) staining kit and Enhanced BCA Protein Assay Kit were purchased from Beyotime Institute of Biotechnology (Shanghai, China). All the other chemicals and reagents used in our experiments were of analytical grade.

## Cell Lines and Animals

HeLa cells (human cervical cancer cell line) were purchased from American Type Cell Culture (ATCC, Rockville, USA), U14 cells (mouse uterine cervix cancer cell line) were provided by Hongshun Biological Technology Co., Ltd. (Shanghai, China).

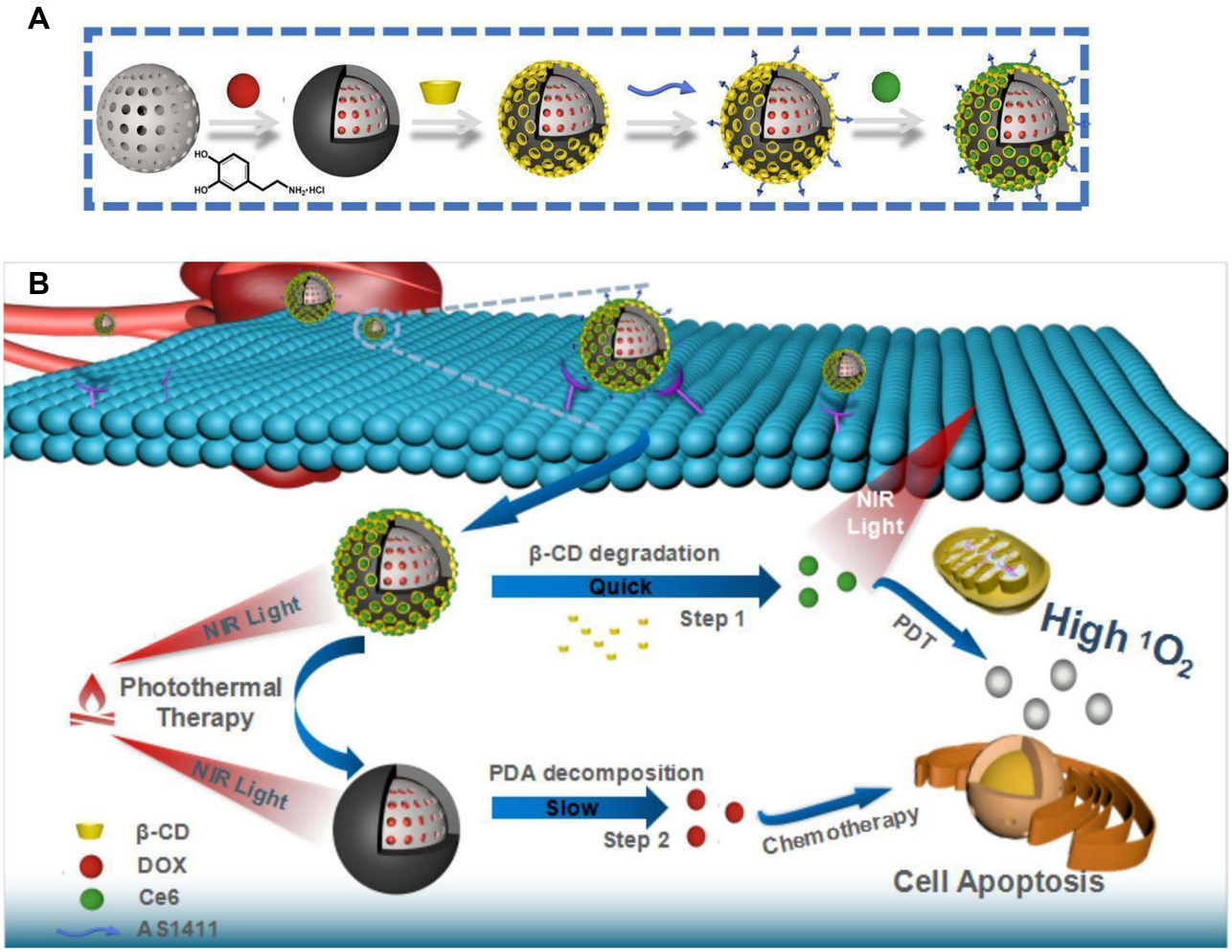


**Scheme 1** (**A**) Synthesis procedure of DOX@MSN@PDA-β-CD/Ce6-AS1411 nanoparticles. (**B**) Function mechanisms of DOX@MSN@PDA-β-CD/Ce6-AS1411 nanoparticles for multimodal synergistic therapy.

4~6-week-old Kunming mice (SPF grade, 20 ± 2 g, female) were purchased from River Laboratory Animal Technology Co., Ltd. (Beijing, China). The animals were maintained in 12-hour-light/-dark cycle and kept at an SPF environment with constant relative humidity (40 ± 10%), room temperature (22 ± 2°C). The animal experiments were conducted according to the National Institutes of Health Guide for the Care and Use of Laboratory Animals and approved by the Animal Care and Use Committee in Yanshan University, China (Ethics number: YD2020022).

## Synthesis of DOX@MSN@PDA-β-CD/Ce6- AS1411

0.5 g CTAB and 0.2 g NaOH were put into a three-mouth flask and then dissolved in 200 mL deionized water combined with ultrasonic for complete dissolution. Next, the solution was mixed under 80°C and 2.4 mL TEOS was added into the solution and stirred further. After the centrifugation (14,000 rpm, 15 min), the precipitation was collected and freeze-dried. Then, the template was removed by condensation reflux method: 50 mL methanol and 2.5 mL HCl (37.5%) were added to the white powder at 65°C for condensation and reflux for 72 h. The obtained product was centrifuged (14,000 rpm, 15 min), dried, and ground to obtain MSN for subsequent experiments.

To load DOX into the channels of MSN, 30 mg MSN and 3.0 mg DOX were dissolved in deionized water and stirred in dark for 12 h to obtain DOX@MSN (DM).

After DM was evenly dispersed in Tris-HCl buffer solution (pH = 10), 20 mg DA-HCl was added and stirred vigorously for 10 h, further centrifuged to obtain DOX@MSN@PDA (DMP).

Next, 5 mg HS-β-CD and DMP were mixed and incubated for 6 h to obtain DOX@MSN@PDA-β-CD (DMPC), then 1 OD $NH_2$-AS1411 was added into DMPC for reacting 4 h at room temperature to synthesize DOX@MSN@PDA-β-CD-AS1411 (DMPCA). Finally, 0.3 mg Ce6 was dissolved in DMSO and further incubated with DMPCA for 4 h in the dark for drug loading to get DOX@MSN@PDA-β-CD/Ce6-AS1411 (DMPCCA) required for the following experiments.

DOX and Ce6 supernatants were collected by centrifugation, respectively, and the absorbance values at 495 nm and 405 nm were measured. Then, the absorbance values were substituted into the standard curve formula to obtain the drug concentration in the supernatant. The drug entrapment efficiency (ER%) and drug loading (DL%) of DOX and Ce6 were calculated by the formula (1) and (2), respectively.

$$ER\% = (Mt - Mf)/Mt \times 100\% \quad (1)$$

$$DL\% = (Mt - Mf)/Mc \times 100 \quad (2)$$

where Mt represents the mass of the total drug, Mf represents the free drug mass in the supernatant, and Mc represents the carrier mass + loaded drug mass.

## Characterization of DMPCCA

BET test was carried out by a specific surface and aperture analyzer (Micromeritics, ASAP 2020 HD88), and the particle morphology was observed by TEM (Talos L120C, USA). The element distribution of the samples was analyzed by energy-dispersive X-ray (EDX) spectra, and the particle size and zeta potential of the samples were detected by Malvern Zetasizer (Nano ZS, Malvern Instrument Co., Ltd., UK). The ultraviolet-visible absorption spectrum of the samples was measured by an ultraviolet-visible spectrophotometer (UV-2550, Shimadzu Co., Ltd., Japan).

## Drug Release Curve in vitro

The drug release kinetics of DMPCCA under different conditions were determined by UV–Vis spectrum combined with the dialysis method. In order to prove the promoting effect of the photothermal conversion of PDA on drug release, four groups of 2 mL DMPCCA solution (1 mg/mL) were placed in dialysis bags for dialysis. The experimental treatment conditions were as follows: PBS solution (pH = 5.0), PBS solution (pH = 7.4), PBS solution (pH = 5.0) + 808 nm laser and PBS solution (pH = 7.4) +808 nm laser. The absorbance values at 495 nm and 405 nm of DOX and Ce6 in dialysate were measured by a multimode microplate reader (Varioskan LUX, Thermo Scientific, USA) and calculated on the basis of the standard curve. Then, the release rate was obtained in accordance with equation (3).

$$Release\% = Mr/Mt \times 100\% \quad (3)$$

Mt represents the total loading mass of the drugs in DMPCCA solution, and Mr stands for the released drug mass in the dialysate.

## Photodynamic Assessment of DMPCCA in Tube

To verify the ROS generation effect of Ce6 loaded in DMPCCA, DPBF was selected as the detection reagent in our experiment.10 μL DPBF (10 μM) solution was added to 90 μL DMPCCA solution (Ce6 concentration in DMPCCA solution was 0.1mg/mL), free Ce6 solution (0.1 mg/mL), and PBS, respectively. Then, all the samples were irradiated under 660 nm (or 808 nm+660 nm) NIR every 1 min, and the fluorescence value of DPBF at 460 nm was measured by a multimode microplate reader (Varioskan LUX, Thermo Scientific, USA).

## Hemolysis Experiment

Hemolysis is a phenomenon of red blood cells rupture and dissolution. Fresh whole blood was obtained from the inferior wing vein of the chicken, and then, red blood cells were isolated by centrifugation. DMPCCA was diluted to the concentration of 31.25, 62.5, 125, 250, 500, and 1000 μg/mL, and the normal saline and distilled water were selected as

negative control and positive control, respectively. 1 mL of 4% (V/V) chicken erythrocyte suspension was added to the different concentrations of DMPCCA solution and control groups, and then, the mixtures were incubated. After centrifugation (5000 rpm, 5 min), the supernatants of different groups were collected. Then, the absorbance at 570 nm of each sample supernatant was detected, and the hemolysis rate of each sample was calculated by the following formula:

$$Hemolysis(\%) = \frac{As - Anc}{Apc - Anc} \tag{4}$$

As, Apc and Anc stand for the absorbance value at 570 nm of DMPCCA-administered samples, positive control treatment sample and negative control treatment sample, respectively.

## Non-Specific Protein Adsorption Experiment

It is necessary to overcome the non-specific protein adsorption of nanoplatforms to achieve effective aggregation at the tumor site, so the non-specific protein adsorption experiment of DMPCCA was conducted. BSA (0.1 mg/mL) was firstly blended with DMPCCA of different concentrations (62.5, 125, 250, 500 and 1000 μg/mL, respectively) and incubated for 10 min. Then, the samples were centrifuged to remove the DMPCCA nanoparticles which might adsorb BSA, and the BCA working solution was added to the supernatant. After incubation for 30 minutes, the absorbance at 560 nm of each sample was measured by a multimode microplate reader (Varioskan LUX, Thermo Scientific, USA).

## In vitro Cytotoxicity Test

CCK-8 kit was used for the cytotoxicity test. Briefly, HeLa cells were inoculated into a 96-well plate and PBS, MSN@PDA-β-CD-AS1411, free DOX, free Ce6, and DMPCCA solutions of specific concentrations were added to each well for 12 h incubation. After irradiation with/without 808 nm and/or 660 nm NIR for 5 min, the cells were incubated for 1 h further, and CCK-8 reagent was added to each well. The absorbance at 450 nm of each sample was read by a multimode microplate reader (Varioskan LUX, Thermo Scientific, USA), and the cell viability was expressed by the following formula.

$$Cell\ viability(\%) = OD_{sample}/OD_{control} \times 100\% \tag{5}$$

The $OD_{sample}$ represents the average absorbance of different test groups at 450 nm, and the $OD_{control}$ represents the average absorbance of the PBS control group at 450 nm.

## Live/Dead Cell Staining

HeLa cells were inoculated into a 24-well culture plate and attached to the climbing sheets. After different drug treatments for 12 h, the cells were irradiated with/without 660nm and/or 808nm NIR laser (50 $mW/cm^2$) for 5min. The culture medium was sucked out after 1 h, then PBS was added to each well to wash for 3 times. Calcein AM and Propidium iodide (PI) were added to the cells and incubated at room temperature (20–25°C) in dark for 10–20 min, then the climbing sheets were observed under a fluorescence microscope (DM4B, Leica, Germany).

## Detection of Intracellular ROS Production

HeLa cells were inoculated into a 24-well plate for attaching to culture slides. DMPCCA was added to cells and incubated for 6 h. To verify the photothermal promotion for Ce6 release, the cells were under irradiation of 808 nm NIR laser (or not under irradiation) for 5min and further under irradiation of 660 nm for 0, 60, 180, and 300 s, respectively. Then, the medium was removed, and the cells were washed with serum-free medium three times. After DCFH-DA incubation for 20 min at 37°C, the slides were placed under a fluorescence microscope for observation (DM4B, Leica, Germany).

## Cellular Uptake Assay

To evaluate the cellular internalization of DMPCCA, DOX was used as the nanoparticle situation marker due to its autofluorescence properties. HeLa cells were inoculated into a 24-well plate for attaching to culture slides. Then,

DMCCA solution was added to each well for the administration, and the slides were stained with DAPI and placed under a fluorescence microscope for observation (DM4B, Leica, Germany).

## In vivo Infrared Thermography

Kunming mice were subcutaneously injected with $2 \times 10^6$ cells on the left axilla. When tumor volumes reached 1000 $mm^3$, DMPCCA solution (1 mg/kg) was injected into U14 tumor-bearing mice by tail vein. 10 min later, the tumor sites of mice were irradiated by 808 nm NIR laser (2 $W/cm^2$) for 5 minutes, and the photothermal images of the irradiated sites were collected by infrared thermal imager (TIX 580, fluke, USA).

To confirm the tumor-targeting efficiency of DMPCCA, the tumor sites and the non-tumor sites on the other side of mice were irradiated by 808 nm laser, and the temperature was recorded by infrared imager (TIX 580, fluke, USA).

## In vivo Antitumor Study of DMPCCA

Firstly, the left forelimb armpit of mice was injected with a normal saline solution containing $1 \times 10^6$ U14 cells for tumor-bearing models' establishment. Then, the inoculated experimental animals were randomly grouped into 8 sets (5 in each set). 24 h later, tail vein injection was conducted (repeat once every two days, 7 times during the whole experiment) and 808 nm NIR irradiation (2 $W/cm^2$, 5 min) or/and 660 nm NIR irradiation (50 $mW/cm^2$, 5 min) were performed on the other day of drug administration. The normal saline was used as the negative control and MSN@PDA-β-CD-AS1411 was chosen as the carrier control. After tumor formation, the maximum and minimum diameters of each tumor in all groups were measured with a Vernier caliper periodically once every two days, and tumor volume was calculated using equation (6). All the experimental mice were treated for 15 days and then euthanized. The heart, liver, spleen, lung, kidney, thymus, and tumor tissues were dissected, weighed, and fixed in formalin. After paraffin embedding, hematoxylin and eosin (H&E) staining was applied to monitor the changes in major organs and tumors after DMCCA administration. The inhibition rate of tumor growth (IRT) and organ coefficient (OC) were expressed in accordance with equations (7) and (8).

$$Vt = \left(L \times W^2\right)/2 \tag{6}$$

$$IRT = \left(1 - \frac{Wd}{W_n}\right) \times 100\% \tag{7}$$

$$OC = W_o/W_b \tag{8}$$

where Vt represents the tumor volume and L and W represent the maximum diameter and minimum diameter of the tumor, respectively. IRT represents the inhibition rate of a tumor. $W_d$ and $W_n$ represent tumor weights of drug administered group and normal saline treatment group, respectively. OC stands for the organ coefficient of the experimental animals, and $W_o$ and $W_b$ represent the organ weight and bodyweight of mice, respectively.

The whole blood of mice in each group was collected to detect the activities of ALT and AST and the levels of CRE and BUN, so as to evaluate the effect of DMCCA treatment on the liver and kidney functions in mice.

## Statistical Analysis

Data were expressed as mean ± standard deviation (M ± SD), and statistical analysis was conducted by GraphPad Prism 8 software (GraphPad Software Inc., La Jolla, CA, USA). Statistical significance was evaluated using the Student's *t*-test when the groups showed different variances. *P* values <0.05 represented statistically significant.

# Results and Discussion

## Synthesis and Characterization of DMPCCA Nanoparticles

The synthesis process of DMPCCA nanoparticles was elucidated in Scheme 1A. MSN was synthesized by a template method, and DOX was loaded in MSN channels further. Next, DA was self-assembled under alkaline conditions to form PDA coating, which was wrapped on the MSN to obtain DOX@MSN@PDA nanoparticles. Then, HS-β-CD was coupled to PDA by Michael addition reaction, and AS1411 was also modified on the surface of PDA by amide reaction, then

DOX@MSN @PDA-β-CD-AS1411 nanoparticles were obtained. Finally, photosensitizer Ce6 was encapsulated into the chambers of β-CD to get DOX@MSN @PDA-β-CD/Ce6-AS1411 nanoparticles.

In order to confirm the successful synthesis of MSN, TEM, BET, and EDS experiments were conducted, respectively. The TEM image in Figure 1A shows that MSN nanoparticles were spherical with uniform size and dispersion, and the particle size was 40 ~ 60 nm and presented the characteristic fingerprint structure of mesoporous silica. Figure 1B and C showed that the specific surface area of MSN was 844.7168 $m^2/g$, the hole size was 1.236741 $cm^3/g$, and the pore size was 5.85636 nm, respectively, which were consistent with the characteristics of mesoporous materials. As shown in Figure 1D, Si (II) and O (III) elements were detected in MSN, further confirming the successful synthesis of MSN.

To further verify the successful synthesis of DMPCCA, the morphology, particle size, and zeta potential were carried out. Figure 1E (left) showed that the DMP nanoparticles were larger smooth spherical structures with the fingerprint pattern on the surface disappearing. It was estimated that the thickness of the PDA shell was 50–55 nm, and the size of DMP was about 180–200 nm. Figure 1E (right) showed that DMPCCA nanoparticles were not smooth on the surface compared with DMP for the connection of β-CD and AS1411. Figure 1F shows that during the synthesis of DMPCCA nanoparticles, the hydrodynamic diameters of these nanoparticles gradually increased for the coating and linking of PDA, β-CD and AS1411 sequentially. Figure 1G shows that the zeta potential gradually enlarged in negative values during the process of DMPCCA synthesis for a large number of -OH groups contained in PDA and β-CD and the phosphate group in AS1411 aptamer.

To determine that β-CD and AS1411 were successfully decorated on the DMP further, EDX and agarose gel electrophoresis experiments were conducted. EDX assay results (Figure 1H) showed that both S and P elements existed in MSN@PDA-β-CD-AS1411 which indicated SH-β-CD and AS1411 were successfully modified to MSN@PDA-β-CD-AS1411. After amide reaction of $NH_2$-AS1411 and MSN@PDA-β-CD, the supernatant and precipitation were collected and electrophoresed. Figure 1I shows that no obvious band was observed for the supernatant, but the brightness of the precipitation was appeared in the sample hole, indicating that AS1411 was successfully and efficiently coupled to MSN@PDA-β-CD.

Finally, we performed a broad-spectrum scanning analysis to prove the successful loading of chemotherapy drug DOX and photosensitizer Ce6. By UV–Vis, DOX showed a characteristic absorption peak near 495 nm, Ce6 presented a characteristic absorption peak at 410 nm and 650 nm. After DOX and Ce6 encapsulation, typical DOX and Ce6 UV–Vis absorption at 495 nm, 410 nm and 650 nm could be observed (Figure 1J), suggesting the successful loading of DOX and Ce6 of DMPCCA.

## Drug Loading and Release of DMPCCA Nanoparticles

The EE and DL of the drugs were determined by the ultrafiltration method, and the concentration of the supernatant was calculated according to the standard curves of DOX and Ce6, respectively. The EE and DL for DOX were 80.33% and 4.57%, for Ce6 were 87.66% and 0.5%, respectively. The high EEs of DOX and Ce6 were due to the high specific surface area of MSN and the existence of a large number of hydrophobic cavities in β-CDs. To further determine the sequential drug release characteristics of nanoparticles in vitro, DMPCCA nanoparticles were placed under different environments (PBS, pH 7.4 or pH5.0) with/without 808 nm NIR laser irradiation. The absorbance of the solution was detected at different time points by the dialysis method, and the drug concentration was obtained by substituting into the standard curve, so as to calculate the drug release rate and draw the drug release curve. As is shown in Figure 2A and B, as expected, sequential release presented between DOX and Ce6, and the release behavior of Ce6 was faster than DOX.

Under neutral (pH 7.4) and acid (pH 5.0) environment conditions, Ce6 presented different release profiles due to β-CD being acid-responsive. The release of Ce6 was accelerated for the thermal generated by PDA promoting the movement of Ce6 molecules (Figure 2A) and reached the burst release peak at 5 h. As for the DOX release profile, there also existed a distinct profile under neutral (pH 7.4) and acid (pH 5.0) environment conditions for PDA coating's acid responsiveness. 808 nm NIR significantly facilitated the release of DOX because the thermal generated by PDA exposure to NIR irradiation also accelerated the movement of DOX molecules and further promoted the release of DOX from MSN channels (Figure 2B). DOX burst release peak appeared at 10 h and there was a 5 h interval time lag between Ce6 and DOX burst release peak (Figure 2C). It was because the acid degradation of β-CD in the outer layer consumed a certain time to further

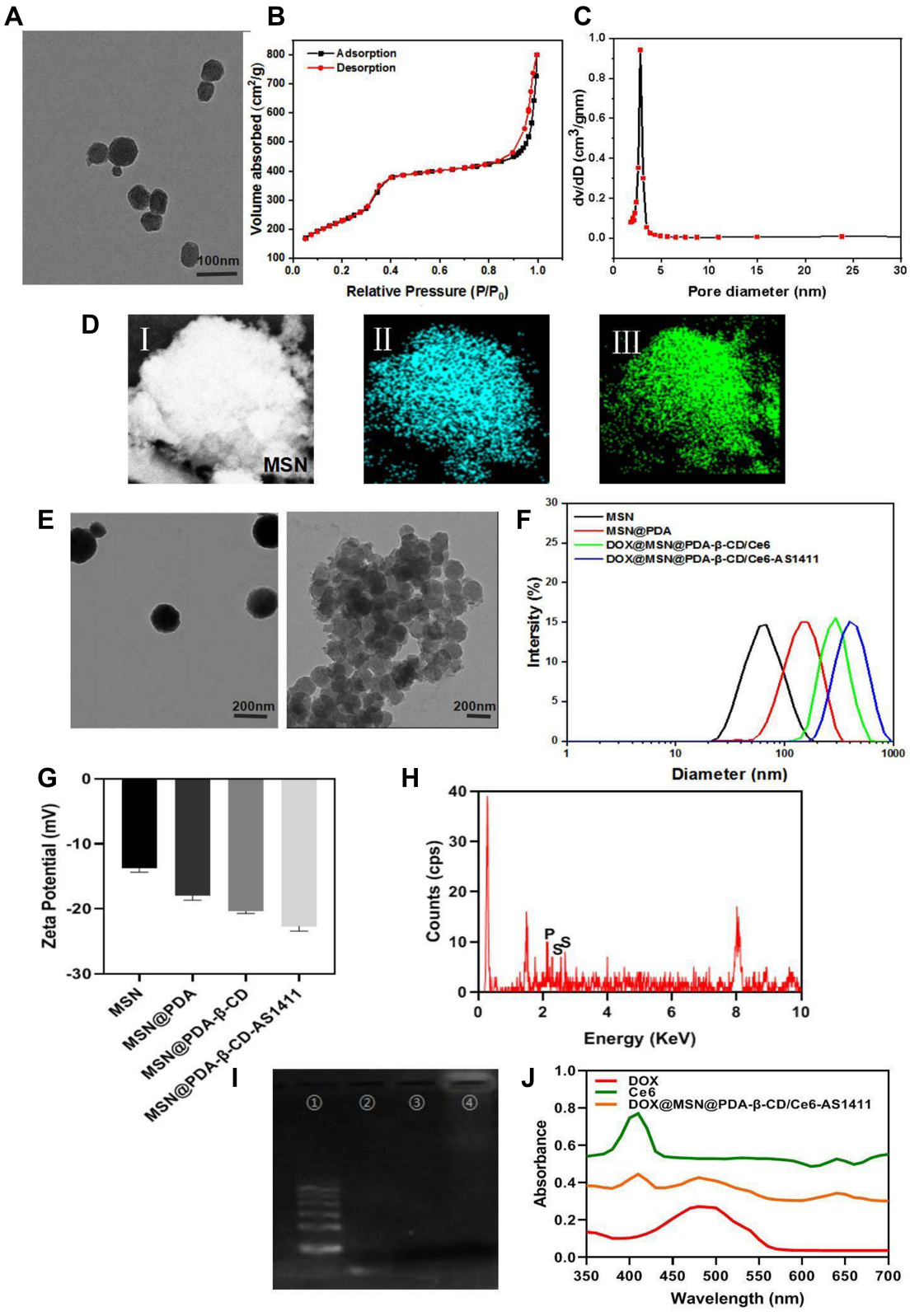


**Figure 1** Synthesis and characterization of MSN and DOX@MSN@PDA-β-CD/Ce6-AS1411. (**A**) TEM images of MSN. (**B**) The pore size distribution of MSN. (**C**) Nitrogen adsorption/desorption isotherm of MSN. (**D**) EDS of Si and O element distribution in MSN. (I: SEM images of MSN. II: EDS of Si element in MSN. III: EDS of O element in MSN.) (**E**) TEM images of MSN@PDA (left) and DOX@MSN@PDA-β-CD/Ce6-AS1411 (right). (**F**) Hydrodynamic size distribution changes during the synthesis process of DOX@MSN@PDA-β-CD/Ce6-AS1411. (**G**) Zeta potential changes during the synthesis process of DOX@MSN@PDA-β-CD/Ce6-AS1411. (**H**) EDX spectrum of MSN@PDA-β-CD-AS1411. (**I**) Agarose gel electrophoresis image of the linking reaction products of AS1411 with MSN@PDA-β-CD. ① marker; ② free AS1411; ③ the supernatant after the reaction of AS1411 with MSN@PDA-β-CD; ④ the reaction products of MSN-PDA-β-CD and AS1411. (j) UV-vis absorbance spectrum of free DOX, free Ce6 and DOX@MSN@PDA-β-CD/Ce6-AS1411.

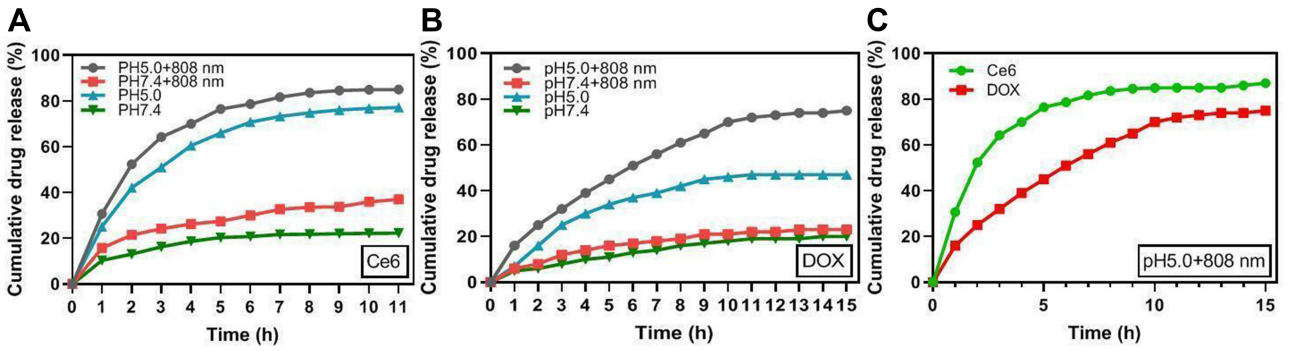


**Figure 2** Drug release profiles of DOX@MSN@PDA-β-CD/Ce6-AS1411 under different conditions. (**A**) Kinetics of Ce6 release from DOX@MSN@PDA-β-CD/Ce6-AS1411 under different conditions. (**B**) Kinetics of DOX release from DOX@MSN@PDA-β-CD/Ce6-AS1411 under different conditions. (**C**) Kinetics of Ce6 and DOX release from DOX@MSN@PDA-β-CD/Ce6-AS1411 under pH5.0+808 nm NIR laser irradiation condition.

acidolysis PDA, and the release of DOX from MSN channels also took a certain time, which forms the sequential release of Ce6 and DOX. Previous studies have shown that PDT therapy could realize cell damage through direct and indirect cytotoxicity by ROS effect, which was produced by light-activated photosensitizers (PSs).[24,25] Moreover, PDT also provides an effective approach to overcome Pg-p mediated MDR towards cancer nanomedicines and increased chemotherapy drug accumulation.[18–26] Therefore, the 5-h release interval could make Ce6 exhibit the PDT effect, further improve the tumor microenvironment, and make the sequentially released DOX achieve a better tumor treatment effect.

## Photothermal Properties of DMPCCA Nanoparticles in vitro

In order to explore the photothermal properties of DMPCCA nanoparticles, a series of experiments were conducted. The infrared imaging results of DMPCCA solution (1 mg/mL) in Eppendorf tubes showed that the solution temperature increased significantly with the extension of NIR 880 nm laser irradiation time. After laser irradiation for 8 min, the solution temperature rose to 62.5°C, while the PBS solution as the control showed no significant temperature changes (Figure 3A). Figure 3B shows that after four on/off cycles of 880 nm NIR irradiation, DMPCCA performed constant photothermal conversion properties, indicating that DMPCCA exhibited ideal photothermal stability. Figure 3C shows that the temperature increased significantly with the increment of the laser irradiation intensity, and the temperature of DMPCCA solution reached 61.7°C with 2 W/cm$^2$ laser irradiation intensity for 5min. Figure 3D shows that the temperature also increased significantly with the DMPCCA concentration increment (0, 0.25, 0.5, 1 and 2 mg/mL). All the results above indicated that DMPCCA nanoparticles possessed an ideal photothermal conversion performance.

## Photodynamic Performance of DMPCCA Nanoparticles

To verify the photodynamic properties of DMPCCA nanoparticles, we selected DPBF as a trapping reagent to detect singlet oxygen ($^1O_2$) produced by different nanoparticles. Results in Figure 4A showed that the scavenging rate of DPBF in the DMPCCA+660 nm treatment group was only 49% at the end of 7 min under 660 nm NIR irradiation. While in the DMPCCA+808 nm +660 nm treatment group, $^1O_2$ produced by Ce6 attenuated DPBF to 81% of the initial value after 7 minutes of irradiation, which was almost equal to the DPBF elimination effect of free Ce6 +660 nm treatment. These results indicated that PDA coating on DMPCCA converted light into thermal after 808 nm irradiation, which further accelerated Ce6 molecules release from β-CDs completely. Then, the liberated Ce6 produced $^1O_2$ and led to the significant scavenge of DPBF after the irradiation of 660 nm NIR. The results above confirmed the ideal photodynamic performance of DMPCCA.

Cytotoxic intracellular ROS related to DNA and mitochondria damages in cells, resulting in cell death, so ROS generation is also a vital indicator for evaluating the performance of PDT. In this study, ROS level was detected by green fluorescence under fluorescent microscopy after 660 nm NIR laser irradiation. Figure 4B shows that with the extension of laser irradiation time, the intracellular fluorescence in both DMPCCA+660 nm treatment cells and DMPCCA+808 nm +660 nm treatment cells increased gradually, indicating that the level of intracellular ROS increased significantly for the

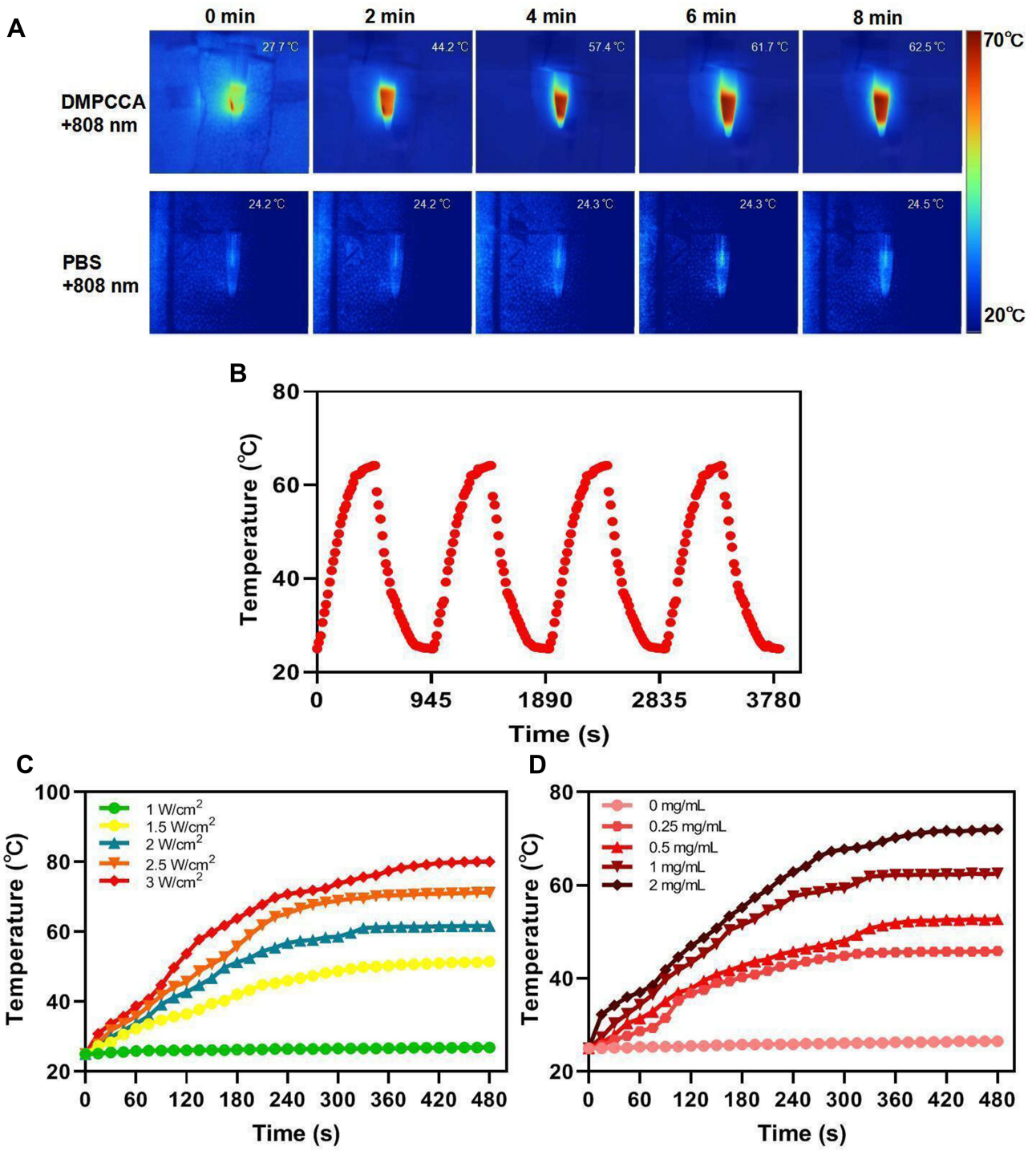


**Figure 3** Photothermal performance analysis of DOX@MSN@PDA-β-CD/Ce6-AS1411. (**A**) Typical thermal images of DOX@MSN@PDA-β-CD/Ce6-AS1411 under 808 nm NIR laser irradiation (2 W/cm$^2$) with different exposure time. (**B**) Temperature record for DOX@MSN@PDA-β-CD/Ce6-AS1411 during four laser "on/off" cycles. (**C**) Photothermal curves of DOX@MSN@PDA-β-CD/Ce6-AS1411 (1 mg/mL) under different powers of 808 nm NIR laser irradiation. (**D**) Photothermal curves of different concentrations of DOX@MSN@PDA-β-CD/Ce6-AS1411 under 808 nm NIR laser irradiation (2 W/cm$^2$).

Ce6 release from DMPCCA under intracellular acidic conditions. The level of ROS in DMPCCA+808 nm+660 nm treatment cells was significantly higher than that in DMPCCA+660 nm treatment cells, indicating that PDA generated thermal and further facilitated the rapid liberation of Ce6 from β-CD cavities, so as to make cells produce more ROS.

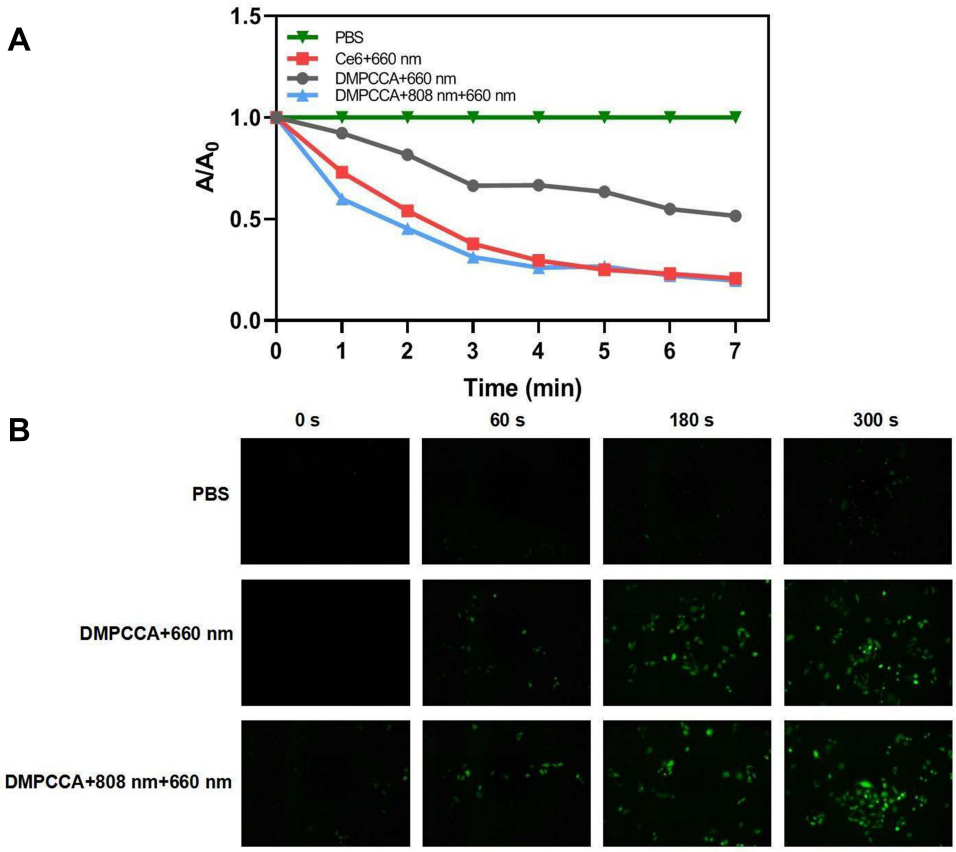


**Figure 4** ROS production assay and cellular uptake of DOX@MSN@PDA-β-CD/Ce6-AS1411 treatment. (**A**) Singlet oxygen generation after treatment of DOX@MSN@PDA-β-CD/Ce6-AS1411 combined with 660 nm and 808 nm laser irradiation sequentially. (**B**) Intracellular ROS generation with the treatment of DOX@MSN@PDA-β-CD/Ce6-AS1411 combined with 660 nm and 808 nm laser irradiation sequentially.

## Cytotoxic Profile of DMPCCA Nanoparticles

To evaluate the cytotoxic effect of DMPCCA on tumor cells, a CCK-8 assay was conducted. As displayed in Figure 5A, MSN@PDA-β-CD-AS1411 manifested no notable cytotoxicity toward HeLa cells, indicating that the drug delivery system itself was harmless to cells. Meanwhile, both free DOX and Ce6+660 nm treatments showed significant cytotoxic effects on HeLa cells for their chemotherapy and PDT on tumor cells ($P<0.001$). DMPCCA+880 nm administration further inhibited the cell growth for the combination of chemotherapy and PTT significantly ($P<0.001$). Interestingly, although DMPCCA+660 nm treatment showed a certain cytotoxic effect on cells ($P<0.01$), its inhibition effect on HeLa cells was rather limited. We speculated that under intracellular acid conditions, Ce6 was released from decomposed β-CDs. However, the release of Ce6 was very sluggish at room temperature, which was due to the incomplete disintegration of β-CD under acidic environment. DMPCCA+808 nm+660 nm administration showed the strongest inhibition effect on HeLa cells for the combination of chemotherapy, PTT, and PDT, in which the heat generated by PDA accelerated the rapid and sequential release of Ce6 and DOX ($P < 0.001$ vs PBS, and $P < 0.01$ vs DMPCCA+660). As shown in Figure 5B, DMPCCA+808 nm+660 nm treatment manifested a dose-dependent cell inhibition effect. With the increase of DMPCCA concentration, the inhibition effects on cell proliferation increased significantly. The above results indicated that DMPCCA+808 nm+660 nm administration combined chemotherapy of DOX, PDT of Ce6 and PTT of PDA together and realized ideal cell proliferation inhibition effect in vitro.

To visualize the chemotherapy-PTT-PDT combination efficacy of DMPCCA nanoparticles, a calcein-AM (green FL, live cells) and PI (red FL, dead cells) co-staining was performed. HeLa cells were treated with PBS, MSN@PDA-β-CD -AS1411,

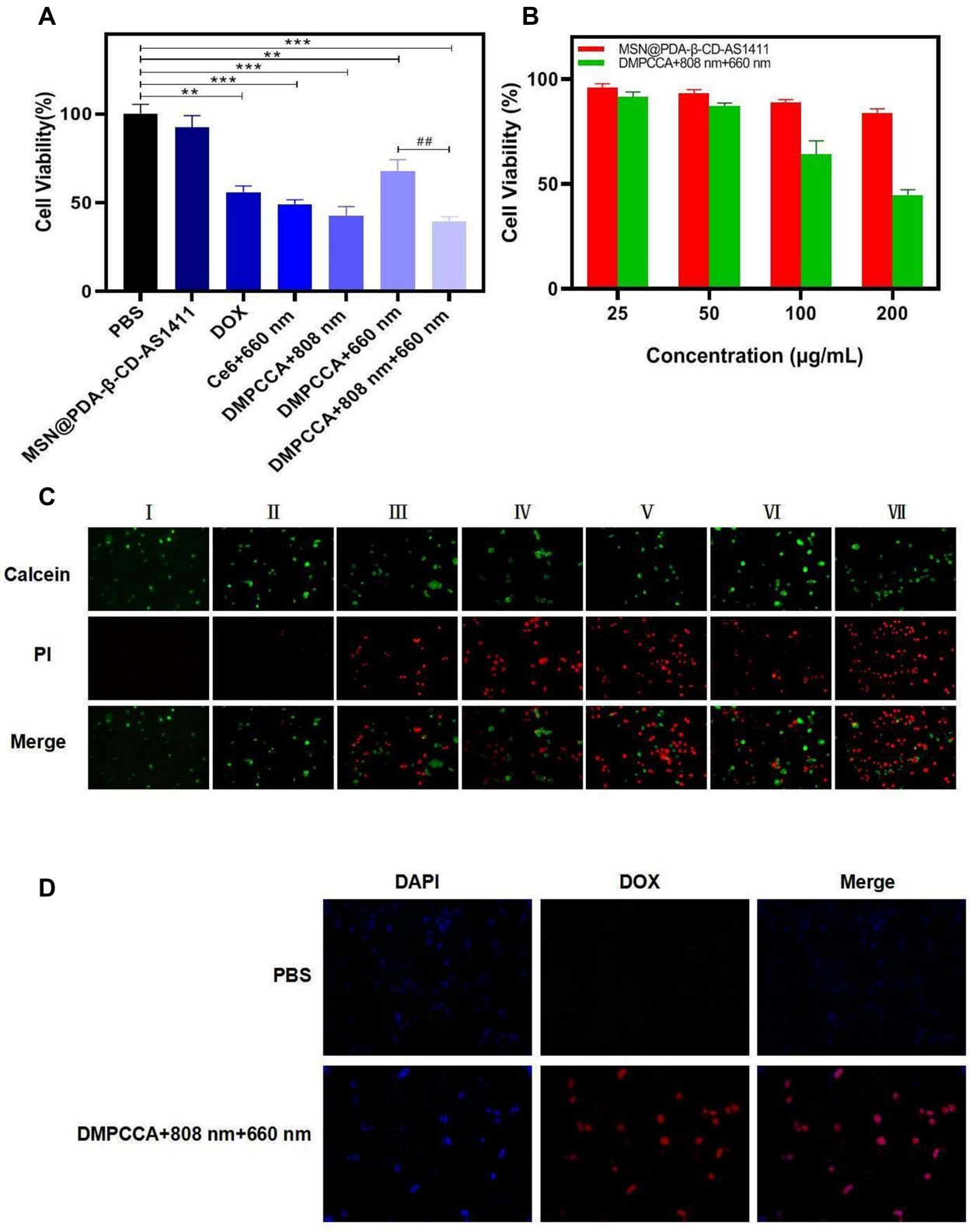


**Figure 5** Cytotoxicity of DOX@MSN@PDA-β-CD/Ce6-AS1411 on Hela cells. (**A**) Cell viabilities of HeLa cells with different treatments. (**B**) Cell viabilities of Hela cells treated with DOX@MSN@PDA-β-CD/Ce6-AS1411 in different concentrations. (**C**) Live/dead cell staining of HeLa cells with different treatments. (**D**) Cellular uptake by DOX@MSN@PDA-β-CD/Ce6-AS1411 treatment. Values represented were means±SD (n=3); $^{**}P<0.01$ or $^{***}P<0.001$, compared with PBS treatment control; $^{\#\#}P<0.01$, compared with DOX@MSN@PDA-β-CD/Ce6-AS1411+660 nm treatment.

**Notes**: I. PBS; II. MSN@PDA-β-CD-AS1411; III. DOX; IV. Ce6+660 nm; V. DMPCCA+808 nm; VI. DMPCCA+660 nm; VII. DMPCCA+808 nm+660 nm.

**Abbreviation**: DMPCCA, DOX@MSN@PDA-β-CD/Ce6-AS1411.

free DOX, Ce6+660 nm, DMPCCA+808 nm, DMPCCA+660 nm, and DMPCCA+808 nm+660 nm, respectively. Figure 5C shows that the blank vector control treatment group induced little cell death, further confirming the safety of this kind of drug delivery system. Free DOX and Ce6+660 nm administrated cells appeared to be more dead cells, for the chemotherapy and PDT induced by DOX and Ce6, respectively. Under 808 nm NIR irradiation, DMPCCA exhibited chemotherapy and PTT combination effect on Hela cells and induced more cell death. Consistent with the results of the CCK-8 assay, DMPCCA+660 nm treatment induced fewer cell death compared with Ce6+660 nm treatment and DMPCCA+808 nm treatment because of the incomplete acid degradation of β-CD, further leading to Ce6 partial release. DMPCCA+808 nm+660 nm treatment induced the most cell death for under 808 nm and 660 nm irradiation sequentially, PDA exerting thermal accelerating the DOX and Ce6 sequential release, realizing chemotherapy, PTT and PDT combination on HeLa cells.

A fluorescence microscope was further used to observe the drug subcellular distribution in cells treated with DMPCCA+808 nm+660 nm. Figure 5D shows that after DMPCCA nanoparticles entered the cells through endocytosis, DOX achieved lysosomal escape successfully under 808 nm and 660 nm irradiation, entered the nucleus further, inhibited DNA and RNA synthesis, and induced cell death. We speculated that Ce6 produced a large number of ROS under 660 nm irradiation, which further cause lysosomal membrane lipid peroxidation and lysosomal escape of DOX.

## Antitumor Efficacy of DMPCCA Nanoparticles in vivo

Encouraged by the superior proliferation inhibition effect on tumor cells of DMPCCA nanoparticles in vitro, we sought to examine their potential for combination therapy in vivo. Firstly, we evaluated the in vivo photothermal performance of DMPCCA under 808 nm irradiation. After mouse cervical cancer U14 cells were inoculated subcutaneously in the armpit of the left forelimb on mice and the tumor volume reached 1000mm$^3$, the DMPCCA solution (78 mg/kg.bw) was injected through the caudal vein and irradiated with 808nm NIR laser 10 min later. The temperature changes of tumor tissue sites were monitored by a thermal imager. Results in Figure 6A manifested the temperature at the tumor site increased significantly with the extension of laser irradiation time. After continuous irradiation for 120 s, the tumor site rose to 52°C. The result above indicated that DMPCCA also possessed ideal photothermal conversion performance in vivo, which could be used for PTT.

To further verify the outstanding tumor-targeting effect of DMPCCA nanoparticles in vivo, 808 nm laser was used to illuminate the tumor site and the non-tumor site on the opposite side after tail vein injection of DMPCCA, and then the thermal imaging images of the irradiated site were captured. Figure 6B shows that the tumor site temperature rose to 52°C after the irradiation for 120 s. While, there were no significant temperature changes after laser irradiation on the contralateral non-tumor site for 120 s. It was because that after DMPCCA entered the circulatory system, more DMPCCA nanoparticles accumulated at the tumor tissue site due to the passive targeting provided by EPR and the active targeting endowed by AS1411. PDA exhibited a photothermal conversion effect, which significantly increased the local temperature of the tumor site. However, there was no obvious drug accumulation in the non-tumor site of the opposite side, resulting in no significant change in temperature. The results confirmed the superior tumor-targeting effect of DMPCCA nanoparticles in vivo.

The U14 tumor-bearing models were established, and the mice were divided into 8 groups randomly (I: Normal saline administrated group, II: free DOX (4 mg/kg.bw) administrated group, III: free Ce6+660 nm administrated group, IV: MSN@PDA-β-CD-AS1411 (78 mg/kg.bw) administered group, V: DMPCCA (78 mg/kg.bw)+808 nm administrated group, VI: DMPCCA (78 mg/kg.bw)+660 nm administrated group, VII: DMPCCA (78 mg/kg.bw)+808 nm +660 nm administrated group, VIII: DMPCC (78 mg/kg.bw) +808 nm +660 nm administrated group). As illustrated in Figures 6C, 7 times of tail vein injection (once every two days) were conducted, and 808 nm illumination and/or 660 nm illumination were performed on the other day of drug injection during the whole experiment, 15 days for the whole experiment. Figure 6D-F shows that in comparison to normal saline administered group, MSN@PDA-β-CD-AS1411 manifested no obvious inhibition efficacy on tumor growth, implying that the vector itself possessed no tumor inhibition effect. DOX, Ce6+660 nm, DMPCCA+808 nm, DMPCCA+660 nm, DMPCCA+808 nm+660 nm and DMPCC+808 nm+660nm treatment groups showed significant tumor growth delay compared with normal saline treatment group (or blank vector control group, $P<0.001$) (IRT was 57.14 ± 4.17%, 54.67 ± 5.22%, 65.98 ± 5.77%, 48.52 ± 6.17%, 93.90 ± 3.14% and 82.84 ± 3.99%, respectively). Nevertheless, among the treatment group above, DMPCCA+660 nm treatment showed the

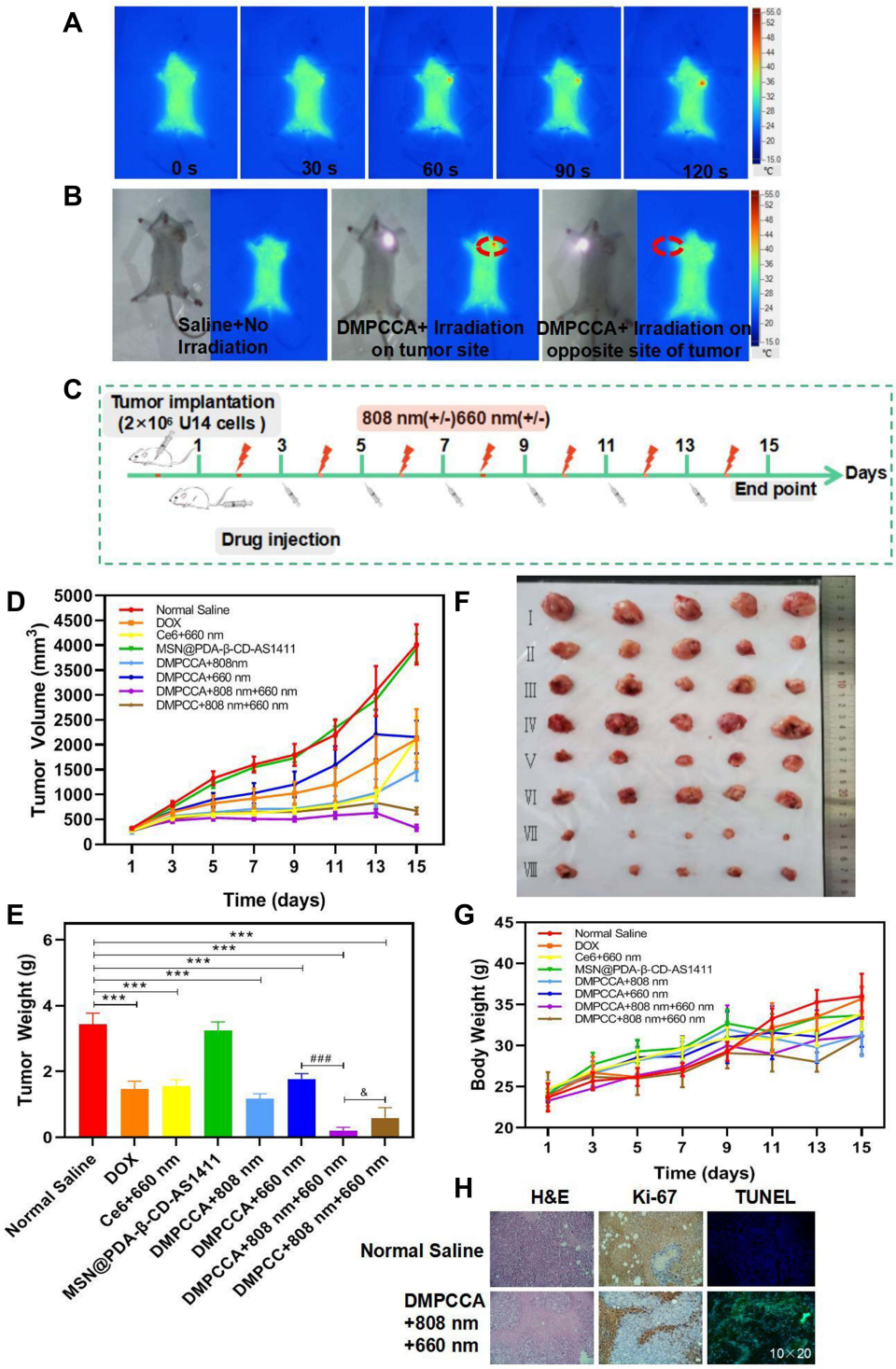


**Figure 6** Antitumor efficacy of DOX@MSN@PDA-β-CD/Ce6-AS1411 in vivo. (**A**) Infrared thermal images of post-injection DOX@MSN@PDA-β-CD/Ce6-AS1411 for different times under 808 nm laser irradiation (2 W/cm$^2$) for 5 min. (**B**) Infrared thermal images of different positions on tumor-bearing mice irradiated by 808 nm laser (2 W/cm$^2$) 10 min after injection of DOX@MSN@PDA-β-CD/Ce6-AS1411. (**C**) Schematic diagram of the therapy schedule on U14 tumor-bearing mice models. (**D**) Tumor volume changes of mice with different therapy procedures. (**E**) Tumor weight of different treatment regimens on the 15$^{th}$ day of the experiment. (**F**) Photographs of isolated tumors of different treatment regimens. (**G**) Body weight changes of mice with different therapy procedures. (**H**) Histopathological observation of tumor sections via H&E staining, Ki-67 IHC staining and TUNEL staining. Values represented were means±SD (n=5); ***P<0.001, compared with Normal saline treatment group; ###P<0.001, compared with DOX@MSN@PDA-β-CD/Ce6-AS1411+660 nm treatment group; &P<0.05 compared with non-AS1411 modified nanoparticles DOX@MSN@PDA-β-CD /Ce6 treatment control.

**Notes**: I. Normal Saline; II. DOX; III. Ce6+660 nm laser; IV. MSN@PDA-β-CD-AS1411; V. DMPCCA+808 nm laser; VI. DMPCCA+660 nm laser; VII. DMPCCA+808 nm +660 nm laser; VIII. DOX@MSN@PDA-β-CD/Ce6+808 nm+660 nm laser.

**Abbreviations**: DMPCCA, DOX@MSN@PDA-β-CD/Ce6-AS1411; DMPCC, DOX@MSN@PDA-β-CD/Ce6.

slightest inhibition effect on tumor growth, which was due to the absence of photothermal conversion of PDA leading to the incomplete Ce6 release from β-CDs. Meanwhile, results of Figure 6D and E also showed that significantly delayed tumor growth and highest tumor inhibition effect (93.90 ± 3.14%) were achieved in DMPCCA+808 nm+660 nm treatment group as compared to the normal saline treatment group, indicating that under double laser irradiation sequentially, the thermal converted by PDA accelerated the Ce6 and DOX sequential release and achieved chemotherapy, PTT and PDT synergy. In addition, this high tumor inhibitory effect of DMPCCA+808 nm+660 nm was also due to the ROS produced by the first released of Ce6, through photodynamic action to inhibit the activity of P-gp protein on the cell membrane, and further increase the concentration in tumor cells of DOX released later. Besides, in order to confirm the active tumor-targeting effect of AS1411 in vivo, the tumor growth in DMPCC + 808 nm + 660 nm administrated group was inspected and further compared with that in DMPCCA + 808 nm + 660 nm administered group. The result showed that compared with the DMPCCA+808 nm + 660 nm administrated group, the tumor growth in the non-AS1411 modified DMPCC + 808 nm + 660 nm administered group was faster ($P<0.05$), implying AS1411 possessed an active tumor-targeting effect and guided more DMPCCA nanoparticles accumulated in tumor tissues.

In addition, during the whole experiment, the changes in body weight, feeding and the behavior status of mice were observed. The results showed that there was no significant difference in mice body weight in DMPCCA + 808 nm + 660 nm administered group (Figure 6G). The feeding and the behavior were normal, indicating that DMPCCA nanoparticles showed no significant systemic toxicity. To disclose the mechanism underlying the superior antitumor effect of DMPCCA + 808 nm + 660 nm administration, the tumor tissues were collected and analyzed. H&E staining results showed that in comparison to the normal saline treatment group, obvious nuclei damages and cytosol degradation existed in the tumor tissues of DMPCCA + 808 nm + 660 nm administered mice. Ki67 IHC staining and TUNEL staining results indicated that DMPCCA + 808 nm + 660 nm administered cells exhibited a high level of apoptosis and a low level of tumor cell proliferation (Figure 6H).

## Biosafety Evaluation of DMPCCA Nanoparticles

Finally, the biosafety of synergistic therapy of DMPCCA + 808 nm + 660 nm was further evaluated. After different medication regimens, mice were sacrificed and the main organs (heart, liver, spleen, lung, kidney, and thymus) were weighed and collected for pathological section preparation. As displayed in Figure 7A, the main organs of DMPCCA + 808 nm + 660 nm treated mice showed no obvious inflammation, cell necrosis, or apoptosis, implying the biosafety of DMPCCA + 808 nm + 660 nm to the main organs in vivo. Furthermore, the organ index presented in Figure 7B showed that there were no significant changes for organ index after different medication regimens, indicating that there was no significant edema in the main organs of mice in each treatment group. A hemolysis assay was then conducted for the detection of hemolytic activity of DMPCCA with different concentrations against RBCs. Results in Figure 7C indicated that up to 1000 μg/mL DMPCCA nanoparticle solution caused no hemolysis, and the hemolysis rates at different concentrations of DMPCCA were all less than 5%, showing that DMPCCA was harmless to erythrocytes. The results of the nonspecific protein adsorption experiment (Figure 7D) showed that different concentrations of DMPCCA exhibited no significant protein adsorption, indicating that DMPCCA nanoparticles possessed no nonspecific protein adsorption ability in blood circulation, which made them escape the scavenging effect of macrophages, show long-term circulation, and accumulate more in tumor tissues through tumor-targeting capacity.

Finally, the biosafety of DMPCCA nanomaterials was evaluated by blood biochemistry tests. Results in Figure 7E showed that there was no significant difference between different medication regimens and normal control groups in CRE, BUN levels and AST/GOT, and ALT/GPT activities. Further confirming that after DMPCCA enters the body by vein injection, 15 days of drug treatment caused no abnormal liver and renal function. Acute toxicity, subacute toxicity test, and tissue distribution test need to be further carried out in our experiment to evaluate the in vivo biosafety of DMPCCA nanoparticles more accurately.

# Conclusion

In summary, we have engineered a novel double-cavity nanocarrier by taking advantage of MSN, β-CD, and PDA. Under the sequential irradiations of double illumination, PDA promoted the extensive release of Ce6 firstly while playing the

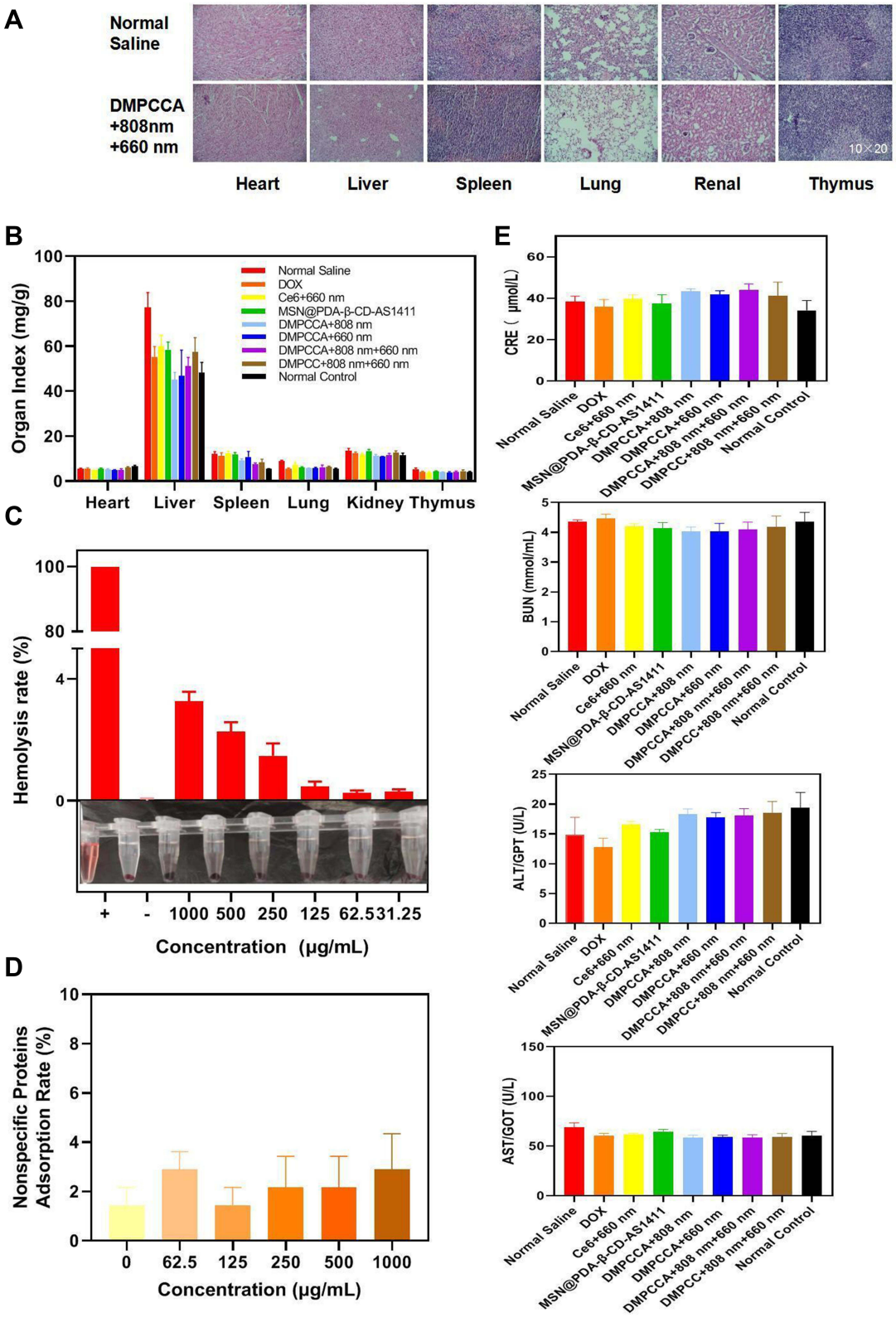


**Figure 7** Biosafety evaluation of DOX@MSN@PDA-β-CD/Ce6-AS1411 in vitro and in vivo. (**A**) Histopathological observation of the main organs via H&E staining. (**B**) Organ indexes of tumor-bearing mice treated with different regimens on the 15th of the experiment. (**C**) Hemolytic percents of chicken erythrocytes incubated with different concentrations of DOX@MSN@PDA-β-CD/Ce6-AS1411. (**D**) Non-specific protein adsorption rates of DOX@MSN@PDA-β-CD/Ce6-AS1411. (**E**) CRE and BUN levels, AST/GOT and ALT/GPT activities in serum of tumor-bearing mice treated with DOX@MSN@PDA-β-CD/Ce6-AS1411. Values represented were means±SD (n=5).sc.
**Abbreviations**: DMPCCA, DOX@MSN@PDA-β-CD/Ce6-AS1411; DMPCC, DOX@MSN@PDA-β-CD/Ce6.

effect of PTT, so as to achieve the effect of PDT. Meanwhile, the rapid release of DOX loaded in MSN channels showed a time lag of about 5 h, through which could maximize the chemotherapeutic effect. Besides, the present drug loading nano platform combined passive tumor-targeting effect given by EPR and active tumor-targeting effect endowed by AS1411 realized PTT-PDT-Chemotherapy triple mode synergistic combination. This study demonstrated a promising nano platform that ensures non-interfering loading and a sequential release of different drugs with different solubilities, which may inspire cancer therapy in the clinic.

## Acknowledgments

This work was supported by the Hebei Natural Science Foundation [grant numbers C2019203556, F2020203056], the National Natural Science Foundation of China [grant number 62071413], Hebei education department key project [grant number ZD2020147], and Hebei Province Key Research and Development Projects in China [grant number 19272401D].

## Disclosure

The authors report no conflicts of interest in this work.

## References

1. Xin L, Huiling S, Wei S, et al. Functionalized poly(pyrrole-3-carboxylic acid) nanoneedles for dual-imaging guided PDT/PTT combination therapy. *Biomaterials*. 2018;167:177–190. doi:10.1016/j.biomaterials.2018.03.030
2. Peng T, Yao H, Xiaoqian F, et al. TPGS/hyaluronic acid dual-functionalized PLGA nanoparticles delivered through dissolving microneedles for markedly improved chemo-photothermal combined therapy of superficial tumor. *Acta Pharm Sin B*. 2021;11(10):3297–3309. doi:10.1016/j.apsb.2020.11.013
3. Cui W, Pengfei W, Zhenpeng H, et al. Construction of surface-modified polydopamine nanoparticles for sequential drug release and combined chemo-photothermal cancer therapy. *Mol Pharm*. 2021;18(3):1327–1343. doi:10.1021/acs.molpharmaceut.0c01164
4. Yuyi L, Xiaobo Z, Yue Z, et al. Activatable photodynamic therapy with therapeutic effect prediction based on a self-correction upconversion nanoprobe. *ACS Appl Mater Interfaces*. 2020;12(17):19313–19323. doi:10.1021/acsami.0c03432
5. Juanjuan D, Hua H, Donglai C, Lichen Y. Manipulating tumor hypoxia toward enhanced photodynamic therapy (PDT). *Biomater Sci*. 2017;5(8):1500–1511. doi:10.1039/C7BM00392G
6. Sepideh A, Navid R, Mojtaba B, et al. Stimulus-responsive sequential release systems for drug and gene delivery. *Nano Today*. 2020;2;34.
7. Ding D, Lixiang W, Yue Q, et al. Non-triggered sequential-release liposomes enhance anti-breast cancer efficacy of STS and celastrol-based microemulsion. *Biomater Sci*. 2018;6(12):3284–3299. doi:10.1039/C8BM00796A
8. Jong-tak L, Jae-Young B. Synthesis and characteristics of double-shell mesoporous hollow silica nanomaterials to improve CO2 adsorption performance. *Micromachines*. 2021;12(11):1424. doi:10.3390/mi12111424
9. Yang B, Yu C, Shi J, et al. Exogenous/endogenous-triggered mesoporous silica cancer nanomedicine. *Adv Healthcare Mater*. 2018;1:1800268. doi:10.1002/adhm.201800268
10. Lijun S. Core-shell hierarchical mesostructured silica nanoparticles for gene/chemo-synergetic stepwise therapy of multidrug-resistant cance. *Biomaterials*. 2017;113:219–228.
11. Palanikumar L, Jeena MT, Kim K, et al. Spatiotemporally and sequentially-controlled drug release from polymer gatekeeper–hollow silica nanoparticles. *Sci Rep*. 2017;7:46540. doi:10.1038/srep46540
12. Hu L, Ma J, Wei X, et al. Biodegradable polydopamine and tetrasulfide bond co-doped hollowed mesoporous silica nanospheres as GSH-triggered nanosystem for synergistic chemo-photothermal therapy of breast cancer. *Mater Des*. 2022;215:110467. doi:10.1016/j.matdes.2022.110467
13. Peng X, Lihong S, Qian L, et al. PEGylated polydopamine-coated magnetic nanoparticles for combined targeted chemotherapy and photothermal ablation of tumour cells. *Colloids Surf B Biointerfaces*. 2017;160:11–21. doi:10.1016/j.colsurfb.2017.09.012
14. Zeng X, Liu G, Tao W, et al. A drug-self-gated mesoporous antitumor nanoplatform based on pH-sensitive dynamic covalent bond. *Adv Funct Mater*. 2017;27(11):1605985. doi:10.1002/adfm.201605985
15. Nicolas B, Thomas L, Feng C, et al. Polyester vascular prostheses coated with a cyclodextrin polymer and activated with antibiotics: cytotoxicity and microbiological evaluation. *Acta Biomater*. 2008;4(6):1725–1733. doi:10.1016/j.actbio.2008.07.001
16. Dongjing Z, Pin L, Cheng Z, et al. Cyclodextrin-based delivery systems for cancer treatment. *Mater Sci Eng C Mater Biol Appl*. 2019;96:872–886. doi:10.1016/j.msec.2018.11.031
17. Pavankumar JB, Britto SS. Programmed and sequential disassembly of multi-responsive supramolecular protein nanoassemblies: a detailed mechanistic investigation. *Chembiochem*. 2021;22(5):876–887. doi:10.1002/cbic.202000581
18. Chengqiong M, Fang L, Yan Z, Waldemar D, Xin M. P-glycoprotein-targeted photodynamic therapy boosts cancer nanomedicine by priming tumor microenvironment. *Theranostics*. 2018;8(22):6274–6290. doi:10.7150/thno.29580
19. Zelai H, Hao J, Xiangyu Z, et al. Nano-delivery vehicle based on chlorin E6, photodynamic therapy, doxorubicin chemotherapy provides targeted treatment of HER-2 negative, alphanubeta3-positive breast cancer. *Pharmacol Res*. 2020;160:105184. doi:10.1016/j.phrs.2020.105184
20. Jianhui Y, Jingxian F, Xiaoling G, et al. Neovasculature and circulating tumor cells dual-targeting nanoparticles for the treatment of the highly-invasive breast cancer. *Biomaterials*. 2017;113:1–17. doi:10.1016/j.biomaterials.2016.10.033
21. Li F, Saisai Z, Xin J, Yongsheng Z, Chaojun S, Hong W. Synergistic chemo-photodynamic therapy by "big & small combo nanoparticles" sequential release system. *Nanomedicine*. 2018;14(1):109–121. doi:10.1016/j.nano.2017.09.002

22. Ma H, He Y, Xu L, et al. Fabrication of polydopamine/hemin-cyclodextrin supramolecular assemblies for mimicking natural peroxidases and their sensitive detection of cholesterol. *J Mol Liq*. 2021;328:115490. doi:10.1016/j.molliq.2021.115490
23. Wang J, Cheng G, Lu J, et al. PDA-cross-linked beta-cyclodextrin: a novel adsorbent for the removal of BPA and cationic dyes. *Water Sci Technol*. 2020;81:11.
24. Zheng H. A review of progress in clinical photodynamic therapy. *Technol Cancer Res Treat*. 2005;4(3):283–293. doi:10.1177/153303460500400308
25. Dennis ED, Dai F, Rakesh KJ. Photodynamic therapy for cancer. *Nat Rev Cancer*. 2003;3(5):380–387. doi:10.1038/nrc1071
26. Li F, Saisai Z, Qian Y, Jiali T, Chaojun S, Hong W. Ternary cocktail nanoparticles for sequential chemo-photodynamic therapy. *J Exp Clin Cancer Res*. 2017;36(1):119. doi:10.1186/s13046-017-0586-1